

PT-Symmetry Enabled Spintronic Thermal Diodes and Logic Gates

Xi-guang Wang, Guang-hua Guo, and Jamal Berakdar*

Devices for performing computation and logic operations with low-energy consumption are of key importance for environmentally friendly data processing and information technology. Here, a design for magnetic elements that use excess heat to perform logic operations is presented. The basic information channel is coupled non-conductive magnetic stripes with a normal metal spacer. The thermal information signal is embodied in magnetic excitations and it can be transported, locally enhanced, and controllably steered by virtue of charge current pulses in the spacer. Functionality of essential thermal logic gates is demonstrated by material-specific simulations. The operation principle takes advantage of the special material architecture with a balanced gain/loss mechanism for magnetic excitation which renders the circuit parity-time symmetric with exceptional points tunable by the current strength in the spacer. Heat flow at these points can be enhanced, be non-reciprocal, or may oscillate between the information channels enabling controlled thermal diode and thermal gate operations. The findings point to a new route for exploiting heat for useful work on the nanoscale.

1. Introduction

The use of excess heat to perform useful operations is a desirable step in developing environmentally friendly devices. To this end, several concepts have been put forward. For instance, phononic-based thermal rectifiers,^[1] thermal diodes,^[2] and thermal logic gates^[3] were proposed as well as thermal transistors.^[4] Furthermore, nano-thermo-mechanical logic gates, three-terminal magnetic thermal transistors,^[5] and flexible thermoelectric switches,^[6] and further thermal-circuit elements^[7–9]

have been demonstrated experimentally. Considering magnetic materials, the low-energy (thermal) excitations that may serve as information carriers are spin waves (or magnons in reference to their excitation quanta). Generally, the utility of magnons for information transmission and processing is endorsed by several experiments, for example, refs. [10–14]. Coherent magnon flow and the input/output signals^[10–21] are controllable by several external parameters, such as magnetic field or spin transfer torques. Material compositions and nano-structuring allow engineering the magnon properties, including their amplitude, phase, dispersion, and signal attenuation.^[10–26]

Magnons can not only be thermally excited, but they can also transport heat as a signal to remote heat-receptive element,^[27–29] which points to the

possibility of magnonic-based thermal signal transfer. Such a possibility is worth investigating in view of the long diffusion length, negligible Joule losses (as opposed to charge current pulses), high frequency, short wavelength (compared to optic-based information processing), and integrability in spintronic devices. Our research presented below indicates that a nonlinear local amplification of magnonic thermal signal is however necessary for realizing thermal logic gates with sufficient fidelity. For this, we exploit a relatively new mechanism for nonlinear signal amplification based on a magnonic realization^[30–32] of parity-time (PT) symmetry.^[33–44] Typically, PT-symmetric systems are coupled to their surroundings and exhibit a transition between the PT-symmetry preserved and broken phases upon changing external parameters. Near the phase-transition (non-Hermitian degeneracy) point, or the exceptional point (EP) the dynamics are highly nonlinear with unique properties such as excitation amplification, enhanced sensitivity to external probes, and non-reciprocity. In our specific case, the magnonic systems are coupled to the surroundings in such a way that the environment-induced magnonic gain and loss are balanced, whilst still realizing a PT-symmetry setup with EPs. Tuning to EPs is accomplished by varying the strength of the balanced gain/loss. How this situation can be realized experimentally is sketched in **Figure 1**: Two insulating magnonic waveguides (WGs) that may exchange power via RKKY or dipolar interactions serve as magnonic couplers^[17–21] for steering signals rendering, for instance, directional coupler or magnonic half-adder.^[16–21]

X.-guang Wang, G.-hua Guo
School of Physics and Electronics
Central South University
Changsha 410083, China

J. Berakdar
Institut für Physik
Martin-Luther Universität Halle-Wittenberg
06099 Halle/Saale, Germany
E-mail: jamal.berakdar@physik.uni-halle.de

 The ORCID identification number(s) for the author(s) of this article can be found under <https://doi.org/10.1002/aelm.202300325>

© 2023 The Authors. Advanced Electronic Materials published by Wiley-VCH GmbH. This is an open access article under the terms of the Creative Commons Attribution License, which permits use, distribution and reproduction in any medium, provided the original work is properly cited.

DOI: 10.1002/aelm.202300325

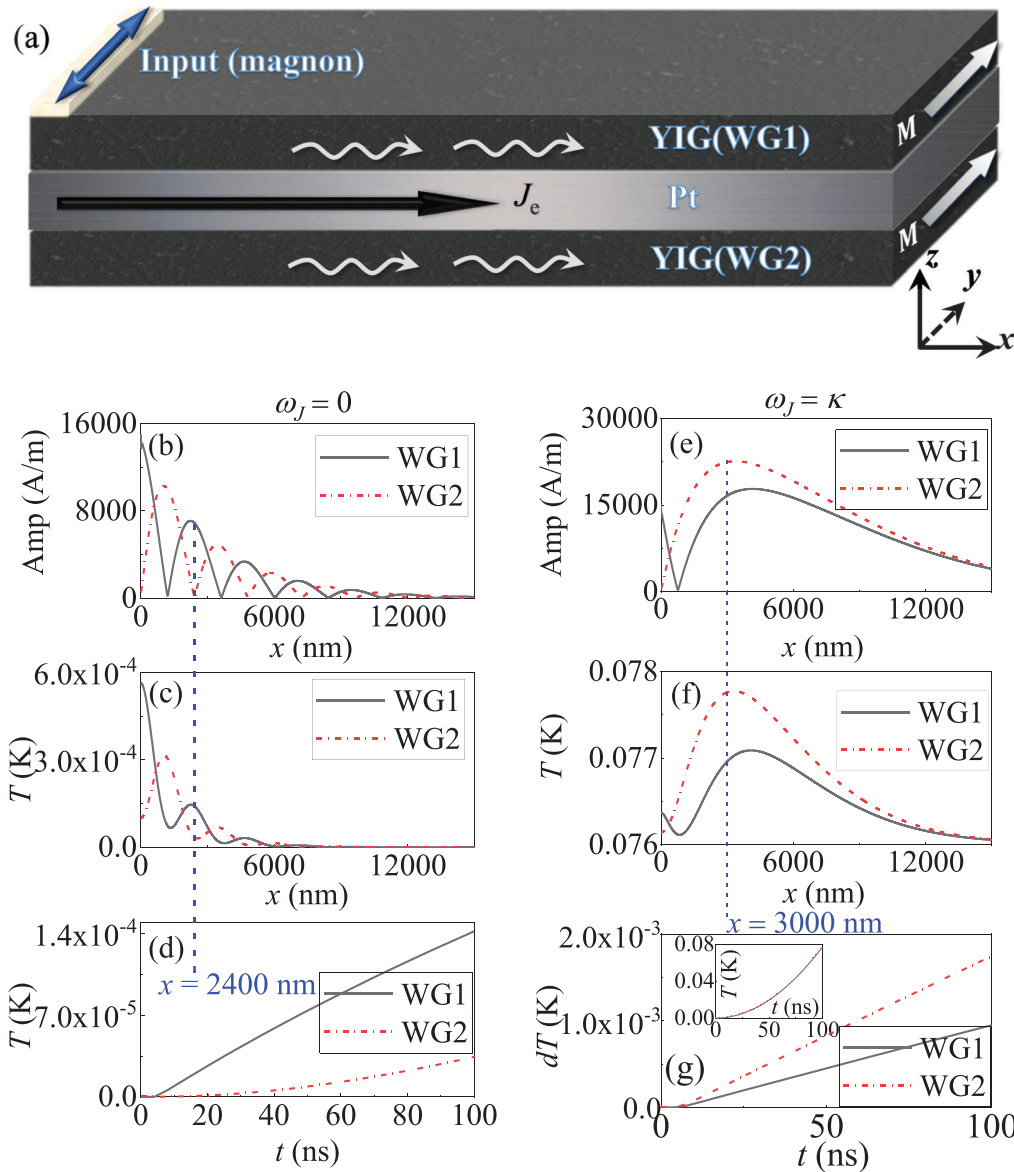


Figure 1. a) Magnetic excitation in two non-conductive magnetic layers serve as planar thermal waveguides (labeled WG1 and WG2) for transmitting information stored in the temperature of local spin excitations. WG1 and WG2 are magnetically coupled with a coupling strength κ . A metallic spacer with a large spin Hall angle is sandwiched between the WGs. Injecting a charge current J_e in the spacer results in opposite spin-Hall torques on the magnetization in WG1 and WG2. The torques damp or antidamp the spin excitations in WG1 and WG2 providing so a balanced gain–loss mechanism (with an effective coupling strength ω_j) and allowing control of the temperature in WG1 and WG2 by varying J_e . Signals are launched locally at the left side of WG1 or WG2 and propagate in both layers. b–d) For $\omega_j = 0$. The signal in WG1 is generated by a local microwave field $h_0 \sin(\omega_h t)$ ($h_0 = 75$ mT and $\omega_h / (2\pi) = 5$ GHz) at $x = 0$. c) The spin excitation temperature after 100 ns. d) Time evolution of the local spin temperature T at $x = 2400$ nm. Switching on J_e such that $\omega_j = \kappa$ changes the (e–g) spatial profiles of the spin excitations amplitude and the induced temperature. g) At $x = 3000$ nm, time evolution of T , and difference $dT = T - T(h_0 = 0)$ between temperatures with and without the microwave field. In all simulations Joule heating due to J_e is included.

Inserting between the WGs a charge-current carrying metallic layer with strong spin orbit coupling results in PT-symmetric magnonic coupler with spin-orbit-torque (SOT) magnonic damping of one WG and equally SOT-antidamping in the other WG. The damping/antidamping is caused by SOT at the interface between the magnetic WG and the normal metal spacer. This structure possesses EPs tunable by the strength of the magnonic gain/loss effect, which is linearly dependent on the charge cur-

rent density in the metal layer. At EPs, the spin dynamics is highly nonlinear.^[30]

So far, the heat associated with the spin-wave dynamics and its possible functionalization in PT-symmetric systems has not been considered. In fact, PT symmetry is usually reported for wave systems and it is more delicate to realize for heat diffusion.^[45] We propose and simulate the heat flow embodied in spin waves that are triggered and propagate in

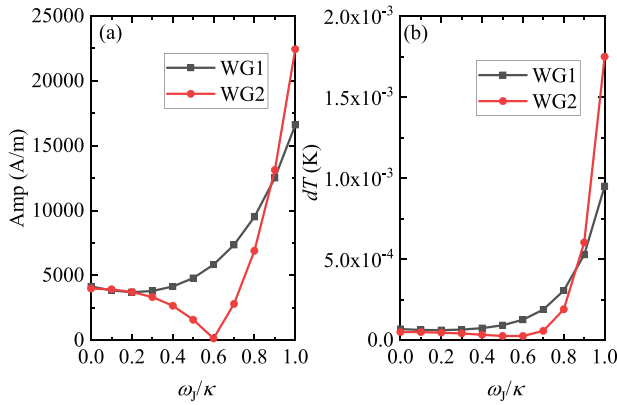


Figure 2. At $x = 3000$ nm, the ω_j dependent spin-wave amplitude and temperature difference $dT = T - T(h_0 = 0)$ between temperatures with and without the microwave field. The spin-wave is excited by a local microwave field $h_0 \sin(\omega_h t)$ ($h_0 = 75$ mT and $\omega_h / (2\pi) = 5$ GHz) at $x = 0$.

magnetic WGs with sandwiched non-magnetic metallic spacers with strong spin-orbit coupling. It is shown how an appropriate design renders the whole structure PT-symmetric and allows for long-distance heat diffusion and control with sufficient fidelity that enables functional thermal logic gates. The existence of EP is important insofar as the spin waves amplitude and the induced heat flow is both enhanced there, while the spin waves can still propagate to a considerable distance and in a non-reciprocal way, which is key to realizing magnonic thermal diodes.

2. Theoretical Model

We study two coupled insulating ferromagnetic waveguides (WG1 and WG2) separated by a charge-carrying spacer with strong spin-orbit coupling; see Figure 1a. To be specific, we use Pt as a spacer layer in the simulations and assume the WGs to be interlayer-exchange coupled, but the conclusions are also valid for other spacer materials and WGs coupling schemes. Yttrium iron garnet (YIG) interfaced with Pt^[46–48] is a prototypical example. We are interested in magnons that transport heat over a remote distance. The WGs magnetic order as well as the launch and propagation of magnons are governed by the Landau–Lifshitz–Gilbert (LLG) equation,^[49,50]

$$\frac{\partial \mathbf{m}_p}{\partial t} = -\gamma \mathbf{m}_p \times (\mathbf{H}_{\text{eff},p} + \mathbf{H}_{\text{th}}) + \alpha \mathbf{m}_p \times \frac{\partial \mathbf{m}_p}{\partial t} + \mathbf{O}_p \quad (1)$$

$p = 1, 2$ enumerates WG1 and WG2. M_s is the saturation magnetization, and \mathbf{m}_p is a unit magnetization vector field. γ is the gyromagnetic ratio and α is the intrinsic (Gilbert) damping constant. The effective field $\mathbf{H}_{\text{eff},p} = \frac{2A_{\text{ex}}}{\mu_0 M_s} \nabla^2 \mathbf{m}_p + \frac{J_{\text{coup}}}{\mu_0 M_s \tau_p} \mathbf{m}_{p'} + H_B \mathbf{y}$ includes contributions from the internal exchange field (exchange constant A_{ex}), the interlayer coupling field (coupling constant J_{coup}), and an external magnetic bias field applied along the y -axis, where $p, p' = 1, 2$ and $p \neq p'$. SOTs $\mathbf{O}_{1(2)} = \gamma c_j \mathbf{m}_{1(2)} \times (+(-)\mathbf{y}) \times \mathbf{m}_{1(2)}$ acting on the two magnetic layers are caused by the charge current in the spacer J_e , resulting in magnonic loss and gain in WG1 and WG2, respectively. The effect of SOT is encapsulated

in $c_j = \theta_{\text{SH}} \frac{\hbar J_e}{2\mu_0 e \tau_p M_s}$, which is proportional to J_e and the spin Hall angle θ_{SH} in the spacer layer.^[49,50]

As for thermal effects, we note that it is possible to generate and measure magnons controllably even at sub-Kelvin temperatures.^[51,52] To capture the influence of the uncorrelated thermal fluctuations on the spin wave dynamics, one may use thermal random magnetic fields with a correlation function $\langle H_{\text{th},q}(r, t) H_{\text{th},q'}(r', t') \rangle = \frac{2\alpha k_B T}{\gamma \mu_0 M_s V} \delta_{qq'} \delta(r - r') \delta(t - t')$. Here, $q, q' = x, y, z$, k_B is the Boltzmann constant, T is the temperature, and V is the volume of the sample. The magnetization-dynamics-induced heating is described by the heat diffusion equation,^[27]

$$\frac{dT_p}{dt} = \frac{1}{c_h \rho} \left[k_t \nabla^2 T_p + \alpha \mu_0 M_s (\mathbf{m}_p \times \frac{d\mathbf{m}_p}{dt}) \cdot \mathbf{H}_{\text{eff},p} + q_{\text{ext},p} \right] \quad (2)$$

where k_t is the thermal conductivity, c_h is the heat capacity, and ρ is the mass density. The α -dependent term quantifies the heat transfer between spin waves and the lattices in WGs due to the damping of the collective spin precession in WGs. The Newton term $q_{\text{ext},p} = c_h \rho \left(\frac{T_0 - T_p}{\tau_1} + \frac{T_{\text{Pt}} - T_p}{\tau_2} \right)$ describes the heat exchange between the sample at temperature T_p , the surroundings at temperature T_0 , and the spacer material Pt at temperature T_{Pt} , where τ_1 and τ_2 are the characteristic thermal relaxation times. The change of temperature T_{Pt} in the spacer Pt (with charge current density J_e leading to heating) is described by,

$$\frac{dT_{\text{Pt}}}{dt} = \frac{1}{c_{h,\text{Pt}} \rho_{\text{Pt}}} \left(k_{t,\text{Pt}} \nabla^2 T_{\text{Pt}} + \frac{J_e^2}{\sigma_{\text{Pt}}} + c_{h,\text{Pt}} \rho_{\text{Pt}} \frac{T_1 + T_2 - 2T_{\text{Pt}}}{\tau_2} \right), \quad (3)$$

Here, σ_{Pt} is the electrical conductivity of Pt.

Solving the three coupled equations (Equations (1)–(3)) allows insight into how heat and spin wave excitation are exchanged between the WGs, spacer, and environment. Generally, experiments with T_0 in mK are possible. T_{Pt} depends on J_e . As demonstrated in ref. [53], the required J_e in our setup can be far below the J_e for auto-oscillations. In the simulations below, we did not optimize the structure to operate at the lowest J_e that could be achieved, such as by nanostructuring the WGs.^[53]

For numerical demonstration, we interfaced Pt with a Yttrium-Iron-Garnet (YIG), meaning $M_s = 1.4 \times 10^5$ A m⁻¹, $A_{\text{ex}} = 3 \times 10^{-12}$ J m⁻¹, $\alpha = 0.005$, $J_{\text{coup}} = 2.1 \times 10^{-6}$ J m⁻². A sufficiently large magnetic field $H_B = 1 \times 10^5$ A m⁻¹ drives the system to the remanent state $\mathbf{m}_{0,p} = \mathbf{y}$. The thermal behavior was solved using $\frac{k_t}{c_h \rho} = 1.5 \times 10^{-6}$ m² s⁻¹, $k_t = 8$ W m⁻¹ K⁻¹, $\tau_1 = 1$ s, and $\tau_2 = 1 \times 10^{-5}$ s. For the Pt spacer, parameters $\frac{k_{t,\text{Pt}}}{c_{h,\text{Pt}} \rho_{\text{Pt}}} = 2.5 \times 10^{-5}$ m² s⁻¹, $k_{t,\text{Pt}} = 71.6$ W m⁻¹ K⁻¹, and $\sigma_{\text{Pt}} = 9.43 \times 10^6$ (Ωm)⁻¹. The size of WG1, spacer, and WG2 adopted in the simulation is $40 \mu\text{m} \times 4 \text{ nm} \times 5 \mu\text{m}$ for a $4 \text{ nm} \times 4 \text{ nm} \times 5 \mu\text{m}$ unit simulation cell. Along the spin-wave and heat-diffusion direction (i.e., the x -axis), the cell size is 4 nm, which is smaller than the exchange length ($\sqrt{\frac{2A_{\text{ex}}}{\mu_0 M_s^2}} = 15.6$ nm), and hence it is found sufficient for capturing correctly the spin-wave propagation and related heating effect. Along the y -direction (the width), the spin-wave is uniformly excited and its propagation is totally suppressed, and thus a $5 \mu\text{m}$ cell size is adopted. For the numerical implementation, we

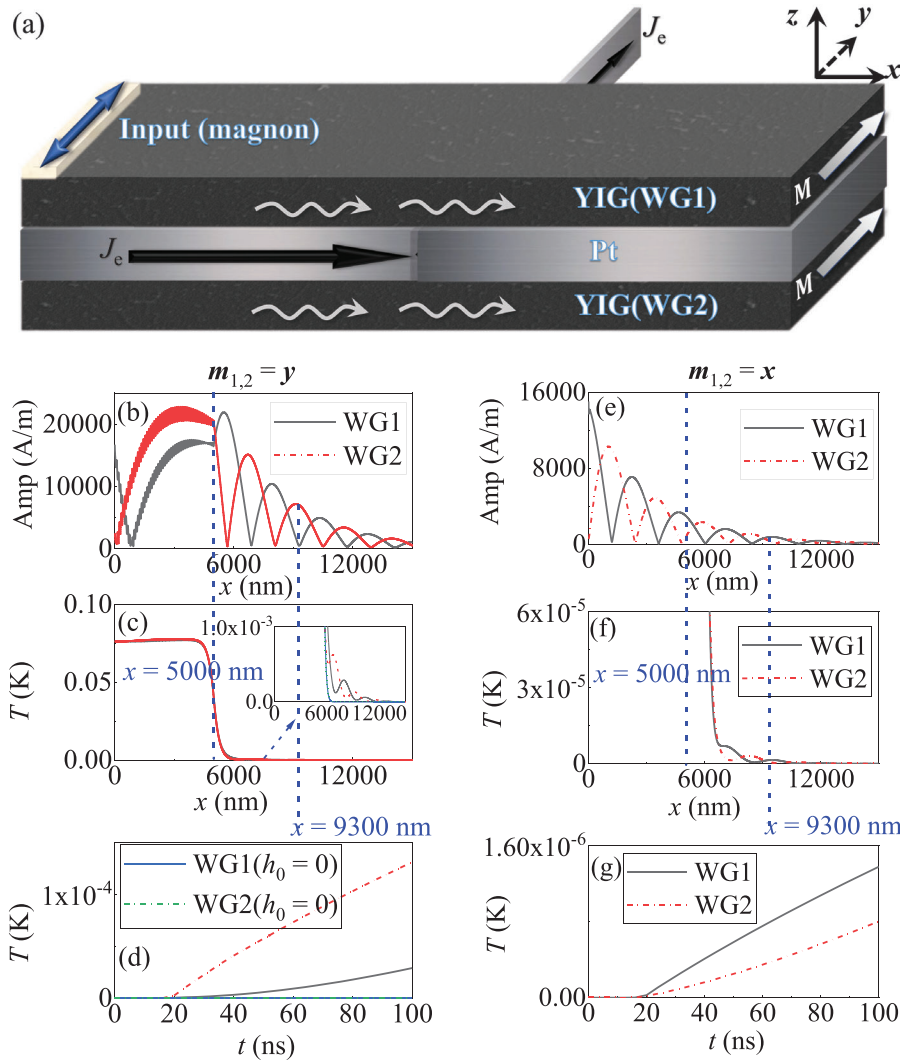


Figure 3. a) The spacer with charge current J_e is only partly attached to the two magnetic layers ($x < 5000$ nm) and the current is diverted out the circuit beyond this region. For $\omega_l = \kappa$, b,c) spatial profiles of magnon amplitudes and induced temperature. Magnons are launched by the local microwave field $h_0 \sin(\omega_h t)$ ($h_0 = 75$ mT and $\omega_h / (2\pi) = 5$ GHz) at $x = 0$ in WG1. d) At $x = 9300$ nm, time evolution of temperature excited by $h_0 = 75$ mT and $h_0 = 0$. e–g) Same curves when the external magnetic field is applied along x .

use the Dormand–Prince method (RK45) with a fixed time step of 0.2 ps, for propagating Equations (1) and (2) self-consistently. The temperature distribution enters as the amplitude of a random field (uncorrelated noise). We checked that if we cut the time step for the simulation by half (then 0.1 ps), no visible changes to the results are found, which ensures the convergence of the results.

3. Results and Discussion

3.1. Magnon Heating Effect in the PT-Symmetric Waveguide

We first analyze the eigen-dynamics of magnons and two eigen-frequencies (optical and acoustic magnon modes) can be obtained as $\omega_{\pm} = (1 - i\alpha)(\omega_0 \pm \sqrt{\kappa^2 - \omega_0^2})$. Here, we introduce $\omega_l = \frac{\gamma c_l}{1 + \alpha^2}$, $\omega_0 = \omega_{\text{ex}} + \kappa$, $\omega_{\text{ex}} = \frac{\gamma}{1 + \alpha^2} (H_B + \frac{2A_{\text{ex}}}{\mu_0 M_s} k_x^2)$ and $\kappa = \frac{\gamma J_{\text{coup}}}{(1 + \alpha^2) \mu_0 M_s \uparrow_p}$.

The opposing spin-orbit torques acting on the adjacent magnetic stripes enhance the spin-wave damping (meaning more loss in spin-wave amplitude) in one waveguide and decrease the magnons in the other waveguide (which means less loss or gain in spin-wave amplitude). Such a coupled gain/loss design is found to lead to antisymmetric imaginary components of the spin-wave potential function, and the whole structure becomes a PT-symmetric system.^[30] Below the gain/loss threshold ($\omega_l < \kappa$), the two optic and acoustic modes are separated. At $\omega_l = \kappa$, two modes coalesce (meaning they become non-Hermitian degenerated), which is the hallmark of the occurrence of an exceptional point (EP). Above the EP ($\omega_l > \kappa$), the real components of ω_{\pm} are still the same (with a small α), and the two imaginary components are separated. Without SOT $\omega_l = 0$, real parts of ω_{\pm} are separated, and two imaginary parts are the same. Exciting two magnon modes with different k_x and the same frequency ω , because of the interference between the two modes, the spin wave

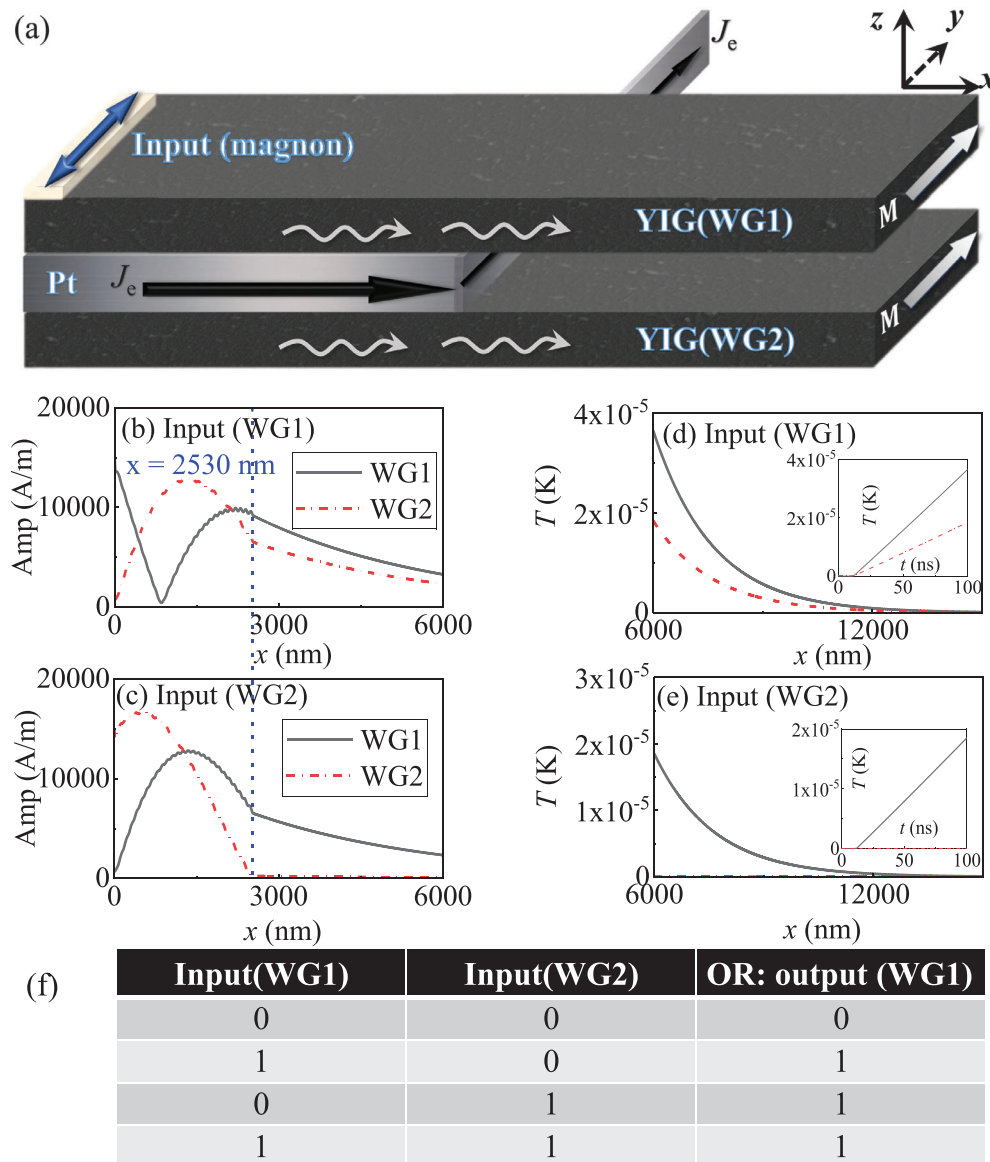


Figure 4. a) The spacer with charge current J_e only acts on the WGs partially ($x < 2530$ nm). b,c) For $\omega_j = 0.7\kappa$, spatial profiles of the magnon amplitudes when the input lies in WG1 or WG2. d,e) Spatial profiles and time evolution (at $x = 6000$ nm) of temperatures heated by magnons in (b,c). f) Logic "OR" operation table.

excited at one end of the waveguide (say WG1) oscillates between WG1 and WG2, as demonstrated in Figure 1b. The induced temperature profile is shown in Figure 1c, and a similar oscillating feature is identified. With time, the magnetization dynamics induced temperature is increases (Figure 1d), and the difference between the two guides originates from the different oscillation amplitudes.

A well-defined EP is identified at $\omega_j = \kappa$ (the corresponding current density $J_e = 6.4 \times 10^6 \text{ A cm}^{-2}$), where two eigenfrequencies coalesce at $\omega_{\pm} = (1 - i\alpha)\omega_0$.^[30] The excited spin waves simultaneously propagate in the two WGs, as seen in Figure 1e. Compared with the case for $c_j = 0$ (Figure 1b), the excited spin wave amplitude becomes much larger and propagates through a much longer distance. For the heating effect, the Joule heat-

ing in the spacer transfers a uniform temperature to neighboring guides. In addition to the uniform Joule heating temperature, the propagating spin waves induce an inhomogeneous T (Figure 1f). Its value is directly determined by spin wave amplitude. The time-dependent temperatures from Joule heating and the magnetization dynamics ($dT = T - T(h_0 = 0)$) are shown in Figure 1g. We note that, due to limited computational resources, our numerical demonstrations are performed for relatively small values of the temperature, and hence, the predicted signal is relatively low. In particular, our simulations are limited to several hundred nanoseconds. Nevertheless, our analysis and results indicate that the spin-wave induced temperature increase is time sustainable. This is important insofar, as in an experimental realization with several milliseconds, a much larger detectable

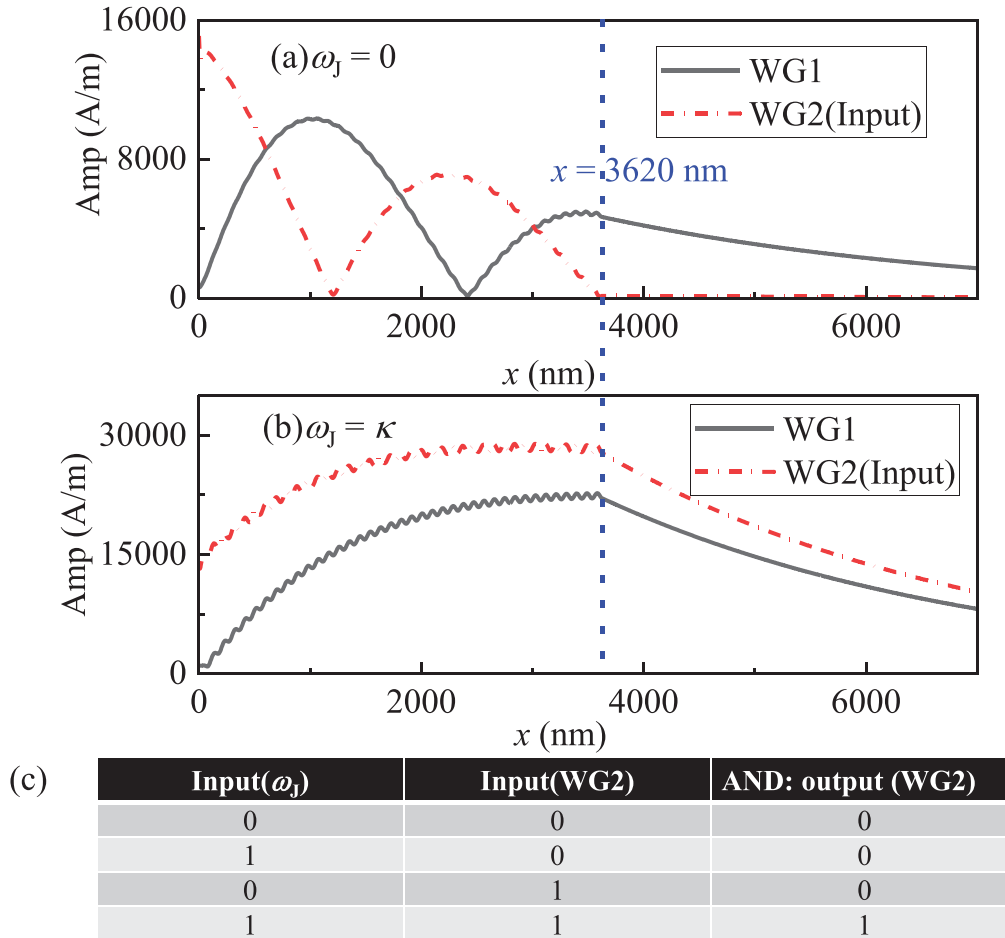


Figure 5. Applying the local microwave field $h_0 \sin(\omega_h t)$ ($h_0 = 75$ mT and $\omega_h/(2\pi) = 5$ GHz) at $x = 0$ in WG2, spatial profiles of magnons for a) $\omega_j = 0$ and b) $\omega_j = \kappa$. c) Logic “AND” operation table based on the results in (a,b). Here, the range with SOTs and interlayer coupling is $x < 3620$ nm.

temperature value is to be expected. On the other side, it should be noted that the operation time of devices based on the scheme presented here will be relatively slow (GHz) but energy-consuming and efficient.

Another conceptual remark concerns the dynamics near the EP: A slight variation in the charge current ω_j strongly changes the spin-waves and related heating effect, that is, the existence of EP leads to enhanced sensitivity, which is crucial for the construction of thermal diodes and gates that operate with sufficient fidelity. An example is seen in Figure 2. With the increase in the electric current term ω_j , the nonlinear enhancement in the spin-wave amplitude and dT are evident, especially around the EP $\omega_j = \kappa$. At $\omega_j = 0.6\kappa$, the spin-wave amplitude in WG2 is suppressed to zero. This is also related to the ω_j induced change in the superposition of two magnon modes, and the spin-wave amplitude minimum point is moved to $x = 3000$ nm in WG2 at $\omega_j = 0.6\kappa$.

Although heating due to magnetization dynamics is much weaker compared to Joule heating, it can transport heat over a very long distance due to the long attenuation length of the spin wave, while Joule heating is localized. To demonstrate this feature, we consider a structure with the Pt spacer partially attached ($0 < x < 5000$ nm) to two WGs (Figure 3a). As shown in Figure 3b, in the range with Pt and SOTs, the excited spin

waves still propagate simultaneously in the two guides. Outside this range, the oscillations of spin wave amplitudes are restored. The temperature induced by Joule heating is strongly localized near the Pt spacer, see Figure 3c, while the spin waves can carry heat over a larger distance. Furthermore, we compare the time-dependent temperatures at $x = 9300$ nm for the cases with and without propagating spin waves (Figure 3d), thus proving this point. We note that the damping constant $\alpha = 0.005$ is used in the current simulation. In a realistic case, its value can be much smaller (two orders of magnitude smaller) and the spin wave can propagate over a much larger distance (several micrometers). We note that the influence of the damping constant α is multifold. On the one hand, the energy transfer between the spin-wave and heat is directly related to the damping term (Equation (2)), and a smaller α decreases the induced temperature amplitude. On the other hand, the spin-wave amplitude can reach a larger distance, enhancing the remote heating effect. Furthermore, similar effects can be achieved for significantly lower Joule heating by designing the WGs such that EPs are reached at lower J_c .^[53]

Changing the direction of the local magnetic field and thus the equilibrium magnetization to x , SOT cannot damp or anti-damp the magnons in this case, and the PT symmetry related phenomena are shut off. This provides a way to manipulate the magnon

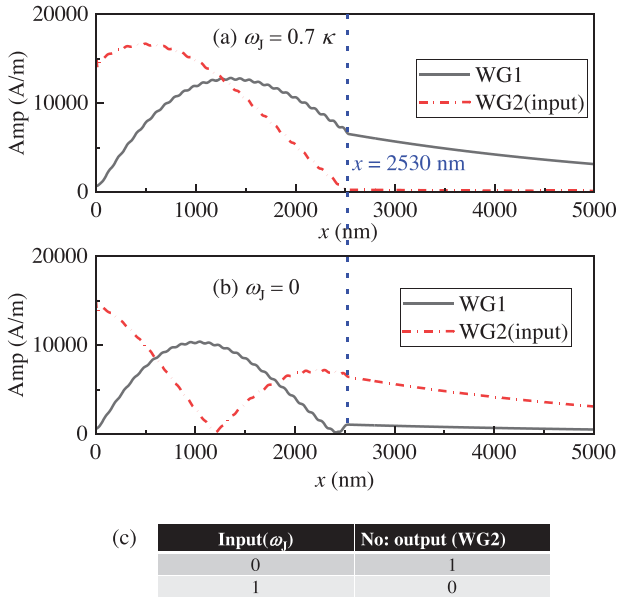


Figure 6. Spatial profiles of magnons for a) $\omega_j = 0.7\kappa$ and b) $\omega_j = 0$. The range with SOTs and interlayer coupling is $x < 2530$ nm. c) Logic “NO” operation table.

induced heat flow using the external magnetic field, as demonstrated by Figure 3e–g. Here, the excited magnon amplitude becomes smaller at $\omega_j = \kappa$, and the related heating effect becomes obviously weaker.

3.2. Heat Diode Design

Our design for a thermal diode is based on non-reciprocal spin wave transfer near the EP. The adopted structure is shown in Figure 4a. In the PT symmetric coupled guides, the non-reciprocal spin wave transfer is led by the superposition of two magnon modes when the charge current $c_j < \kappa$ is smaller than EP. As demonstrated by Figure 4b,c, the magnon amplitudes emitting from the coupling range with charge current ($x < 2530$ nm) become completely different by switching the input (microwave field) from WG1 to WG2. Especially for input in WG2, the emitting magnons are mainly located in WG1, while the amplitude in WG2 approaches zero, which leads to a non-reciprocal heat flow, that is, a realization of a thermal diode, as demonstrated by Figure 4d,e. The time-dependent temperature T is shown in the insets of Figure 4d,e, exhibiting the characteristic features of the thermal diode.

Based on the thermal diode above, we designed several possible logic operations. The logic “OR” operation can be realized in the heat diode structure, as demonstrated by Figure 4f. Here, the input (magnon excited by a microwave field) in WG1 or WG2 is treated as logic “1,” and the nonzero output magnon amplitude in WG1 represents logic “1.” Only in the case without any input in WG1 and WG2, the logic output in WG1 is “0.” Otherwise, the output is always logic 1, meaning a logic “OR” operation between the two inputs (WG1 and WG2).

The logic “AND” operation can be realized in a similar structure, as demonstrated in Figure 5a–c. Here, $\omega_j = \kappa$ and input in

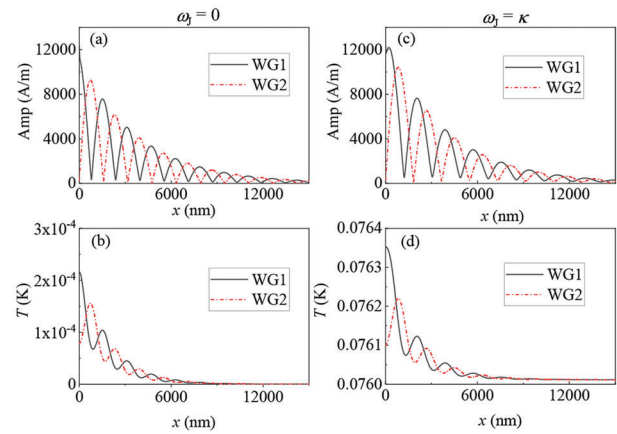


Figure 7. The results of the simulations for the cases depicted in Figure 1a including the dipolar interactions. a,b) For $\omega_j = 0$ and c,d) $\omega_j = \kappa$, the spatial profiles of spin-wave amplitude and induced temperature. The signal in WG1 is generated by a local microwave field $h_0 \sin(\omega_p t)$ ($h_0 = 75$ mT and $\omega_p/(2\pi) = 5$ GHz) at $x = 0$. The spacer with charge current J_e acts on the whole WGs.

WG2 are treated as logic “1,” and the nonzero output magnon amplitude in WG2 is logic “1.” Only for $\omega_j = \kappa$ with input in WG2, the logic output in WG2 is “1,” meaning a logic “AND” operation is realized. The logic “NO” operation is demonstrated in Figure 6. Electric current input $\omega_j = 0.7\kappa$ is logic “1.” Keeping the magnon input in WG2, the output in WG2 is “0” when $\omega_j = 0.7\kappa$. Switching off the electric current, the output becomes “1.” Noteworthy, for the above operations based on PT-symmetric structure, by varying the amplitude of the charge current, we can further dynamically switch between these logic functions.

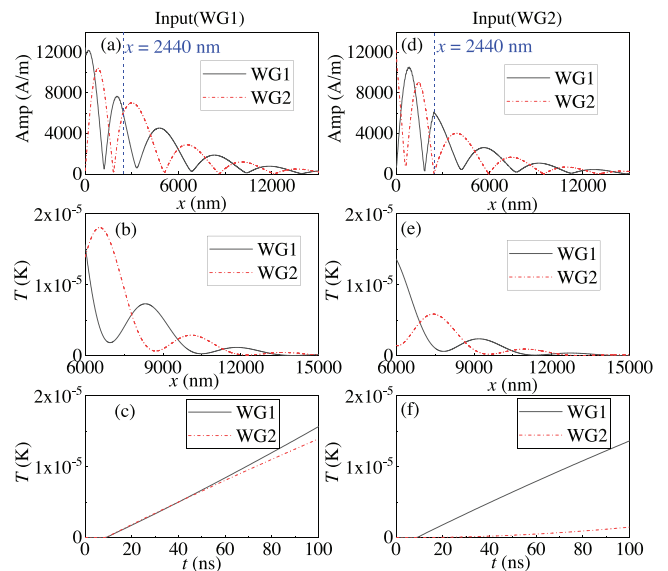


Figure 8. Simulation results for the case of Figure 4a while including the dipolar interactions. When the input lines in a–c) WG1 or d–f) WG2, the magnon amplitudes profile (a,d), temperature profile (b,e), and time-dependent temperature at $x = 6000$ nm (c,f). The spacer with charge current J_e ($\omega_j = \kappa$) acts on the WGs partially ($x < 2440$ nm).

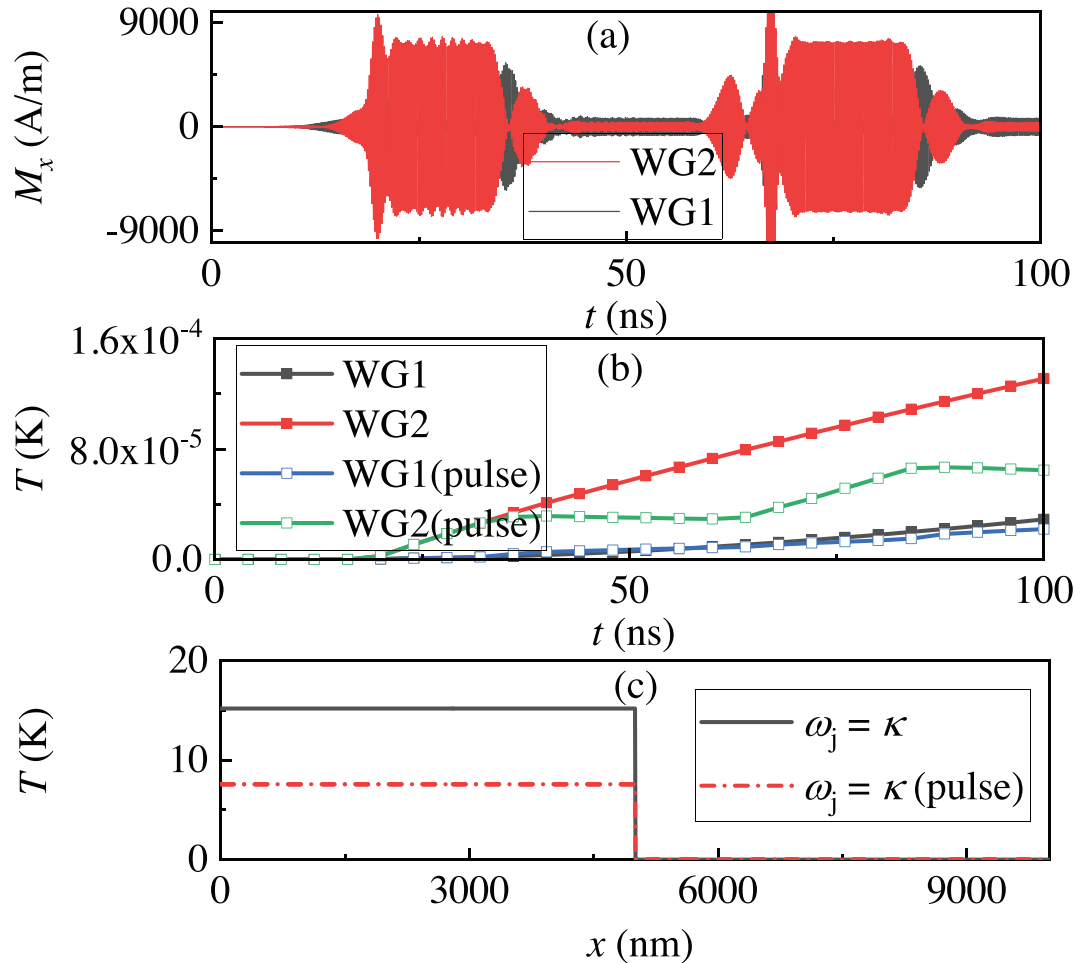


Figure 9. Driven by continuous electric current and pulsed electric current with $\omega_j = \kappa$, a) time dependent M_x detected at $x = 9300$ nm in WG1 and WG2. b) At $x = 9300$ nm, time dependent temperature T . c) Temperature profile in the spacer between WG1 and WG2 at time $t = 100$ ns.

For an experimental realization, it is important to quantify the influence of dipolar interactions. Including the dipolar interaction fields $\mathbf{H}_{\text{demag}}$, we performed simulations for coupled nanostripes. The size of the stripes is as before, namely $40 \mu\text{m} \times 4 \text{nm} \times 5 \mu\text{m}$. The dipolar interaction field $\mathbf{H}_{\text{demag}}$ reads

$$\mathbf{H}_{\text{demag}}(\mathbf{r}) = -\frac{M_s}{4\pi} \int_V \nabla \nabla' \frac{1}{|\mathbf{r} - \mathbf{r}'|} \mathbf{m}(\mathbf{r}') d\mathbf{r}' \quad (4)$$

The results confirm the persistence of the oscillating behavior for the case without electric current $\omega_j = 0$ in **Figure 7a,b**. Due to that, the dipolar interaction increases the coupling between WG1 and WG2, at $\omega_j = \kappa$ (the exceptional point (EP) for the case without dipolar interaction), there is still SW amplitude oscillation as the EP ($\omega_j > \kappa$) is increased by the dipolar interaction (**Figure 7c,d**). Here the spin-wave transfer is non-reciprocal, and one can realize a similar design for the diode and the logic gates. As an example, in **Figure 8**, when the charge current $\omega_j = \kappa$ is locally applied in the range of $x < 2440$ nm (same as the model of **Figure 4a**), we obtain different spin-wave amplitudes outside this range. We note that due to the dipolar interaction, the SW power periodically transfers between the two WGs in the range without

interlayer coupling ($J_{\text{coup}}(x > 2440 \text{ nm}) = 0$). Switching the input from WG1 to WG2, the temperature T near the position $x = 6 \mu\text{m}$ (i.e., output) becomes completely different (**Figure 8c,f**), enabling the possibilities of thermal diode and logic “OR” operation similar to the findings in **Figure 4**.

3.3. Electric Current Pulse and Local Temperature Gradient

To decrease the overall energy consumption of the logic operations, we apply a charge current pulse $J_c(t)$. For a sequence of charge currents with a period of 50 ns (**Figure 9**), the Joule heating induced temperature is decreased by factor 2, compared to DC J_c . When the charge current is switched on, magnons are enhanced (**Figure 9a**), and the enhancement disappears soon when the current is switched off. It also affects the magnon induced heating in two guides. Under the pulsed current, the heating effect becomes obvious weaker compared to that for continuous current (**Figure 9b**). The enhanced nonlinearity of the magnetization dynamics at EPs is favorable for speeding up the logic gate operations. The degree of nonlinearity can be increased by

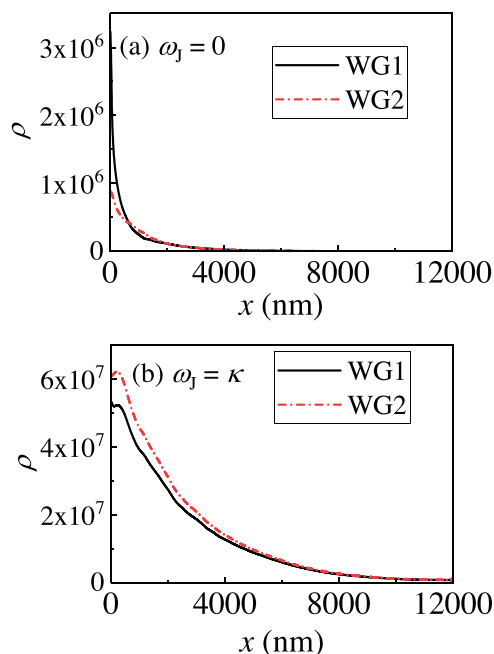


Figure 10. With a) $\omega_j = 0$ and b) $\omega_j = \kappa$, spatial profile of the magnon density $\rho = M_x^2 + M_z^2$. Here, a local temperature 100 K is set at the left end in WG1 ($x < 40$ nm).

having higher-order EPs which can be achievable through WGs design, as demonstrated in ref. [32].

The propagating magnons can be excited via the temperature gradient. Here, we set a local temperature, $T = 100$ K at the left end, and thermally excited magnons propagate toward the rest part of the sample. As demonstrated in **Figure 10a**, thermal magnons can transmit into neighboring WGs via coupling. As thermal magnon frequencies lie in a wide range and the magnon beating length changes with frequency, we do not observe a clear periodic energy transfer between the two guides. Applying $\omega_j = \kappa$, magnons with all frequencies reach EP simultaneously, and there is still an obvious magnon enhancement in the two guides, see **Figure 10b**.

3.4. Relaying Magnon Propagation

To relay the propagating magnons in the WGs, we apply a second microwave field to both WGs. As shown in **Figure 11**, when $\omega_j = 0$, in WG1 the magnon amplitude changes with the phase angle θ of the second microwave field, while in WG2 it remains unaffected. Here, the range with interlayer coupling is $x < 3620$ nm, and without the second microwave field, the emitting magnons mainly distribute in WG1 (**Figure 5a**). At $x = 14\,000$ nm, the amplitude in WG1 is 200 A m^{-1} . With the magnons excited by the second microwave field, the interference between two magnon currents induces the θ dependence amplitude. For $\theta = 1.55\pi$, the larger amplitude in WG1 is kept, and the absolute values of magnon amplitudes in both WG1 and WG2 are increased. Furthermore, when $\omega_j = \kappa$, the emitted magnons distribute over the two WGs and the second microwave field can equally enhance the magnon amplitude in WG1 and WG2 for $\theta = 0.1\pi$.

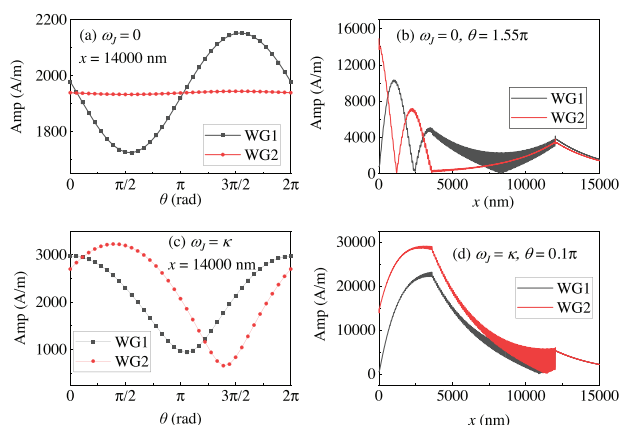


Figure 11. Magnons are injected via applying the local microwave field $h_0 \sin(\omega_h t)$ ($h_0 = 75$ mT and $\omega_h / (2\pi) = 5$ GHz) at $x = 0$ in WG2. At $x = 12\,000$ nm, a second microwave field $h_1 \sin(\omega_h t + \theta)$ ($h_1 = 37.5$ mT) is applied to both guides to relay the injected magnons. a,c) The phase θ dependence of magnon amplitude at $x = 14\,000$ nm when $\omega_j = 0$ or κ . b,d) The spatial profiles of magnon amplitudes. Here, the range with SOTs and interlayer coupling is $x < 3620$ nm.

Here, interference can affect the magnon amplitudes of the two WGs.

4. Conclusion

The medium for the thermal information signals is magnons in coupled PT-symmetric non-conductive magnetic stripes. PT-symmetry is essential to have an EP (or non-Hermitian degeneracy point) at which the information signals can be amplified or steered controllably. The PT-symmetry is brought out by a balanced gain and loss of magnonic excitations due to SOTs at the interface between the spacer and magnetic stripes. A charge current pulse sets the value of the SOT. The current-induced Joule heating is strongly localized. The heat flow associated with magnons can propagate through a long distance (compared to phononic thermal flow), allowing for remote thermal information exchange. The charge current strength tunes the device to the non-reciprocal heat flow regime, which is necessary for thermal diodes enabling several types of reconfigurable logic operations. The results demonstrate an example of PT symmetry in heat diffusion and point to new designs of heat devices.

Acknowledgements

This work was supported by the DFG through SFB TRR227 and Project No. 465098690, the National Natural Science Foundation of China (Grants No. 12174452, No. 12074437, No. 11704415, and No. 11674400), the Natural Science Foundation of Hunan Province (Grants No. 2022JJ20050, No. 2021JJ30784, and No. 2020JJ4104), and the Central South University Innovation-Driven Research Programme (Grant No. 2023CXQD036).

Open Access funding enabled and organized by Project DEAL.

Conflict of Interest

The authors declare no conflict of interest.

Data Availability Statement

The data that support the findings of this study are available from the corresponding author upon reasonable request.

Keywords

heat flow, parity-time-symmetry, spin orbit torque, spin waves, thermal logic gates, unconventional computing

Received: May 24, 2023
Revised: September 7, 2023
Published online: October 4, 2023

- [1] M. Terraneo, M. Peyrard, G. Casati, *Phys. Rev. Lett.* **2002**, *88*, 094302.
- [2] B. Li, J. Lan, L. Wang, *Phys. Rev. Lett.* **2005**, *95*, 104302.
- [3] L. Wang, B. Li, *Phys. Rev. Lett.* **2007**, *99*, 177208.
- [4] B. Li, L. Wang, G. Casati, *Appl. Phys. Lett.* **2006**, *88*, 143501.
- [5] L. Castelli, Q. Zhu, T. J. Shimokusu, G. Wehmeyer, *Nat. Commun.* **2023**, *14*, 393.
- [6] T. da Câmara Santa Clara Gomes, N. Marchal, F. Abreu Araujo, L. Piraux, *Adv. Mater. Technol.* **2022**, *7*, 2101043.
- [7] C. W. Chang, D. Okawa, A. Majumdar, A. Zettl, *Science* **2006**, *314*, 1121.
- [8] T. Ishibe, T. Kaneko, Y. Uematsu, H. Sato-Akaba, M. Komura, T. Iyoda, Y. Nakamura, *Nano Lett.* **2022**, *22*, 6105.
- [9] Y. Zhang, Q. Lv, H. Wang, S. Zhao, Q. Xiong, R. Lv, X. Zhang, *Science* **2022**, *378*, 169.
- [10] V. V. Kruglyak, S. O. Demokritov, D. Grundler, *J. Phys. D: Appl. Phys.* **2010**, *43*, 264001.
- [11] A. A. Serga, A. V. Chumak, B. Hillebrands, *J. Phys. D: Appl. Phys.* **2010**, *43*, 264002.
- [12] A. V. Chumak, V. I. Vasyuchka, A. A. Serga, B. Hillebrands, *Nat. Phys.* **2015**, *11*, 453.
- [13] A. V. Chumak, A. A. Serga, B. Hillebrands, *Nat. Commun.* **2014**, *5*, 4700.
- [14] B. Lenk, H. Ulrichs, F. Garbs, M. Münzenberg, *Phys. Rep.* **2011**, *507*, 107.
- [15] M. Krawczyk, D. Grundler, *J. Phys.: Condens. Matter* **2014**, *26*, 123202.
- [16] A. V. Sadovnikov, E. N. Beginin, S. E. Sheshukova, D. V. Romanenko, Y. P. Sharaevskii, S. A. Nikitov, *Appl. Phys. Lett.* **2015**, *107*, 202405.
- [17] Q. Wang, P. Pirro, R. Verba, A. Slavin, B. Hillebrands, A. V. Chumak, *Sci. Adv.* **2018**, *4*, e1701517.
- [18] Q. Wang, M. Kewenig, M. Schneider, R. Verba, F. Kohl, B. Heinz, M. Geilen, M. Mohseni, B. Lägél, F. Ciubotaru, C. Adelman, C. Dubs, S. D. Cotofana, O. V. Dobrovolskiy, T. Brächer, P. Pirro, A. V. Chumak, *Nat. Electron.* **2020**, *3*, 765.
- [19] A. V. Sadovnikov, A. A. Grachev, E. N. Beginin, S. E. Sheshukova, Y. P. Sharaevskii, S. A. Nikitov, *Phys. Rev. Appl.* **2017**, *7*, 014013.
- [20] Z. Ren, S. Liu, L. Jin, T. Wen, Y. Liao, X. Tang, H. Zhang, Z. Zhong, *Sci. Rep.* **2019**, *9*, 7093.
- [21] X.-g. Wang, L. Chotorlishvili, G.-h. Guo, J. Berakdar, *Phys. Rev. Appl.* **2019**, *12*, 034015.
- [22] A. V. Sadovnikov, C. S. Davies, V. V. Kruglyak, D. V. Romanenko, S. V. Grishin, E. N. Beginin, Y. P. Sharaevskii, S. A. Nikitov, *Phys. Rev. B* **2017**, *96*, 060401.
- [23] M. Vogel, R. Aßmann, P. Pirro, A. V. Chumak, B. Hillebrands, G. von Freymann, *Sci. Rep.* **2018**, *8*, 11099.
- [24] M. Mohseni, R. Verba, T. Brächer, Q. Wang, D. A. Bozhko, B. Hillebrands, P. Pirro, *Phys. Rev. Lett.* **2019**, *122*, 197201.
- [25] L. J. Cornelissen, B. J. van Wees, *Phys. Rev. B* **2016**, *93*, 020403.
- [26] V. E. Demidov, S. Urazhdin, A. Anane, V. Cros, S. O. Demokritov, *J. Appl. Phys.* **2020**, *127*, 170901.
- [27] N. Perez, L. Lopez-Diaz, *Phys. Rev. B* **2015**, *92*, 014408.
- [28] T. An, V. I. Vasyuchka, K. Uchida, A. V. Chumak, K. Yamaguchi, K. Harii, J. Ohe, M. B. Jungfleisch, Y. Kajiwara, H. Adachi, B. Hillebrands, S. Maekawa, E. Saitoh, *Nat. Mater.* **2013**, *12*, 549.
- [29] O. Wid, J. Bauer, A. Müller, O. Breitenstein, S. S. P. Parkin, G. Schmidt, *Sci. Rep.* **2016**, *6*, 28233.
- [30] X.-g. Wang, G.-h. Guo, J. Berakdar, *Nat. Commun.* **2020**, *11*, 5663.
- [31] X.-G. Wang, G.-H. Guo, J. Berakdar, *Appl. Phys. Lett.* **2020**, *117*, 242406.
- [32] X.-g. Wang, G.-h. Guo, J. Berakdar, *Phys. Rev. Appl.* **2021**, *15*, 034050.
- [33] L. Feng, Z. J. Wong, R.-M. Ma, Y. Wang, X. Zhang, *Science* **2014**, *346*, 972.
- [34] M.-A. Miri, A. Alù, *Science* **2019**, *363*, eaar7709.
- [35] Z. Lin, H. Ramezani, T. Eichelkraut, T. Kottos, H. Cao, D. N. Christodoulides, *Phys. Rev. Lett.* **2011**, *106*, 213901.
- [36] L. Feng, Y.-L. Xu, W. S. Fegadolli, M.-H. Lu, J. E. B. Oliveira, V. R. Almeida, Y.-F. Chen, A. Scherer, *Nat. Mater.* **2013**, *12*, 108.
- [37] M. Brandstetter, M. Liertzner, C. Deutsch, P. Klang, J. Schöberl, H. E. Türeci, G. Strasser, K. Unterrainer, S. Rotter, *Nat. Commun.* **2014**, *5*, 4034.
- [38] B. Peng, S. K. Özdemir, F. Lei, F. Monifi, M. Gianfreda, G. L. Long, S. Fan, F. Nori, C. M. Bender, L. Yang, *Nat. Phys.* **2014**, *10*, 394.
- [39] H. Xu, D. Mason, L. Jiang, J. G. E. Harris, *Nature* **2016**, *537*, 80.
- [40] H. Hodaie, A. U. Hassan, S. Wittek, H. Garcia-Gracia, R. El-Ganainy, D. N. Christodoulides, M. Khajavikhan, *Nature* **2017**, *548*, 187.
- [41] T. Yu, H. Yang, L. Song, P. Yan, Y. Cao, *Phys. Rev. B* **2020**, *101*, 144414.
- [42] H. Liu, D. Sun, C. Zhang, M. Groesbeck, R. Mclaughlin, Z. V. Vardeny, *Sci. Adv.* **2019**, *5*, eaax9144.
- [43] A. Galda, V. M. Vinokur, *Sci. Rep.* **2019**, *9*, 17484.
- [44] D. Zhang, X.-Q. Luo, Y.-P. Wang, T.-F. Li, J. Q. You, *Nat. Commun.* **2017**, *8*, 1368.
- [45] Y. Li, Y.-G. Peng, L. Han, M.-A. Miri, W. Li, M. Xiao, X.-F. Zhu, J. Zhao, A. Alù, S. Fan, C.-W. Qiu, *Science* **2019**, *364*, 170.
- [46] R. O. Serha, D. A. Bozhko, M. Agrawal, R. V. Verba, M. Kostylev, V. I. Vasyuchka, B. Hillebrands, A. A. Serga, *Adv. Mater. Interfaces* **2022**, *9*, 2201323.
- [47] L. Liu, Y. Li, Y. Liu, T. Feng, J. Xu, X. R. Wang, D. Wu, P. Gao, J. Li, *Phys. Rev. B* **2020**, *102*, 014411.
- [48] S. Emori, A. Matyushov, H.-M. Jeon, C. J. Babroski, T. Nan, A. M. Belkessam, J. G. Jones, M. E. McConney, G. J. Brown, B. M. Howe, N. X. Sun, *Appl. Phys. Lett.* **2018**, *112*, 182406.
- [49] I. N. Krivorotov, N. C. Emley, J. C. Sankey, S. I. Kiselev, D. C. Ralph, R. A. Buhrman, *Science* **2005**, *307*, 228.
- [50] M. Collet, X. de Milly, O. d'Allivy Kelly, V. V. Naletov, R. Bernard, P. Bortolotti, J. Ben Youssef, V. E. Demidov, S. O. Demokritov, J. L. Prieto, M. Muñoz, V. Cros, A. Anane, G. de Loubens, O. Klein, *Nat. Commun.* **2016**, *7*, 10377.
- [51] S. O. Demokritov, V. E. Demidov, O. Dzyapko, G. A. Melkov, A. A. Serga, B. Hillebrands, A. N. Slavin, *Nature* **2006**, *443*, 430.
- [52] I. V. Borisenko, B. Divinskiy, V. E. Demidov, G. Li, T. Nattermann, V. L. Pokrovsky, S. O. Demokritov, *Nat. Commun.* **2020**, *11*, 1691.
- [53] X.-g. Wang, D. Schulz, G.-h. Guo, J. Berakdar, *Phys. Rev. Appl.* **2022**, *18*, 024080.